An Interaction-Aware Lane Change Behavior Planner for Automated Vehicles on Highways Based on Polygon Clipping

Article *in* IEEE Robotics and Automation Letters · February 2019

DOI: 10.1109/LRA.2019.2898093

CITATIONS
12

READS
286

6 authors, including:

Manuel Schmidt
Technische Universität Dortmund
8 PUBLICATIONS **17** CITATIONS
SEE PROFILE

Carlo Manna
Flemish Institute for Technological Research
9 PUBLICATIONS **24** CITATIONS
SEE PROFILE

Torsten Bertram
Technische Universität Dortmund
287 PUBLICATIONS **2,393** CITATIONS
SEE PROFILE

An Interaction-Aware Lane Change Behavior Planner for Automated Vehicles on Highways based on Polygon Clipping

Manuel Schmidt[1], Carlo Manna[2], Jan Braun[1], Christian Wissing[2], Manoj Mohamed[2] and Torsten Bertram[1]

***Abstract*—This contribution presents A-D-PolyC (Automated Driving using Polygon Clipping), a novel framework for lane change behavior planning of automated vehicles on highways. It assumes that a mission planning layer generates lane change requests. In crowded traffic scenes, various variants for the lane change execution arise. The developed algorithm identifies the maneuver variants deterministically and in bounded runtime using polygon clipping in spatiotemporal domain. The variants are represented using a graph that captures the scene topology. Afterward, it efficiently samples optimal lateral and longitudinal trajectories with regards to vehicle dynamics. The satisfaction of hard constraints is checked. Finally, a scene prediction is conducted for a subset of the sampled trajectories. In comparison with most state of the art approaches, the framework accounts for traffic interaction and collects meaningful features. A novel measure based on generalized kinetic energies for the impact of a maneuver execution on the whole traffic scene is introduced. A-D-PolyC is a hierarchical, holistic, modular and parallelizable concept that can be coupled with different scene prediction engines and lower-level local trajectory planners. The performance of A-D-PolyC is statistically evaluated using randomized simulation runs and compared to a state of the art approach.**

***Index Terms*—Motion and Path Planning, Intelligent Transportation Systems, Computational Geometry, Automated Vehicles, Optimization and Optimal Control**

I. Introduction

AUTOMATED driving has the potential to dramatically reduce fatalities and exceed human capabilities. Furthermore it enables disabled people to regain their individual mobility. Some of the most important aspects in automated driving are the mission planning, scene prediction, behavior and motion planning. Mission planning systems aim to calculate certain waypoints along a route and generate lane change requests based on the infrastructure and maps. The scene prediction answers the question of how a traffic scene will evolve in the near future. In this contribution, behavior planning represents the process of identifying all execution variants of a requested lane change, assessing them and selecting one. Finally, the goal of motion planning is to generate a drivable and collision-free trajectory to conduct the instructions given by the behavior planning. The transition between behavior and motion planning is very fluent. In this architectural view, the behavior planning basically serves as the globalization strategy for the local lower-level motion planning. Often, the interplay of the individual parts is neglected. A-D-PolyC serves as the connecting link between the mission planning, scene prediction and motion planning. It takes into account the various execution variants of lane changes and the influence each variant has onto the surrounding traffic. A-D-PolyC has bounded runtime, uses ideas from computer graphics and most computationally expensive steps can be parallelized.

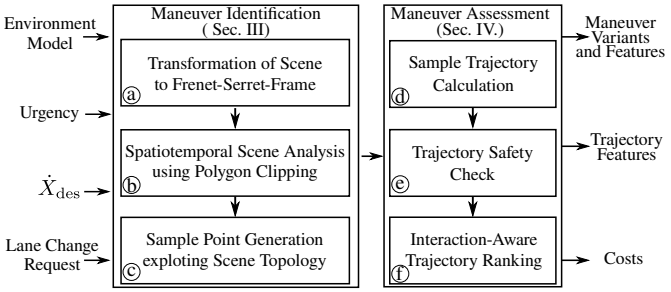

Fig. 1: Overview of the current architecture of A-D-PolyC.

Fig. 1 shows a high-level overview of A-D-PolyC's architecture. Assumed is the knowledge of an environment model that consists of the description of surrounding traffic participants, their predictions and lane marking information. It is invoked by a lane change request that is issued by the mission planning together with the desired velocity $\dot{X}_{\mathrm{des}}$ and the urgency of the lane change. It is more urgent if for example the current lane that is driven on ends soon. Then all maneuver variants are identified using three steps denoted with the letters ⓐ, ⓑ and ⓒ in the Fig. 1. In step ⓐ, the whole traffic scene is transformed into a Frenet-Serret coordinate frame. Then the scene is analyzed in spatiotemporal (L, t) domain using polygon clipping (step ⓑ). Herein, L represents the longitudinal coordinate and t the time. This results in polygons with specific attributes as explained later in section III, especially III-C. Next the polygons are used to efficiently sample points (step ⓒ) for the trajectory calculation (step ⓓ). After obtaining the trajectories, several constraint checks are conducted in step ⓔ. Finally, an interaction-aware trajectory ranking is done in step ⓕ. It is realized by estimating the influence of each maneuver variant onto the surrounding

Manuscript received: September, 10, 2018; Revised December, 02, 2018; Accepted January, 30, 2019.

This letter was recommended for publication by Associate Editor N. Amato and Editor A. M. Okamura upon evaluation of the reviewers' comments.

*This work was supported by ZF Group - TRW Automotive GmbH Düsseldorf, Germany.

[1]Manuel Schmidt, Jan Braun and Torsten Bertram are with the Institute of Control Theory and Systems Engineering, TU Dortmund University, D-44227 Dortmund, Germany. manuel3.schmidt@tu-dortmund.de

[2]Carlo Manna, Christian Wissing and Manoj Mohamed are with ZF Group - TRW Automotive GmbH, Active & Passive Safety Technology, D-40547 Düsseldorf, Germany. carlo.manna@zf.com

Digital Object Identifier (DOI): see top of this page.

traffic. A-D-PolyC currently outputs the maneuver variants, their associated spatiotemporal features and all features as well as the assigned costs of the calculated trajectories.

II. Related Work and Contribution

Many scientific contributions inspired our development. The work [1] introduces the Frenet-Serret-Frame and algorithms for obtaining a C^1-transformation from a global coordinate frame to the Frenet-Serret-Frame. This transformation is used in step ⓐ of A-D-PolyC. Several general formalisms for maneuver variant identification are introduced in [12] for the use in spatiotemporal domain. The approach of [2] was our main inspiration and presents a method for sampling trajectories efficiently by inverting occupancies of lanes to obtain the lanes free spaces in spatiotemporal domain. The interaction-aware components of A-D-PolyC are based on the works of [3] and [4] that both use forward simulations of the traffic scene to assess the influences of trajectories to surrounding traffic. However, both don't exploit the full finite number of emerging maneuver variants and their sampling is therefore more incomplete compared to ours. The scene prediction in A-D-PolyC uses a forward simulation based on the Intelligent Driver Model [13]. A comparison of several state of the art approaches for lane change and general motion planning is shown in table I. The distinguishing features are the maximum planning horizon, interaction-awareness, the globalization strategy and finally the optimization method for obtaining trajectories. A-D-PolyC differs from most of the reported approaches because of the interaction-awareness. Of all sampling-based interaction-aware methods, ours is the only one that uses informed sampling. This means that the traffic scene topology is taken into account for distribution of samples and thus trajectory generation.

There are four main scientific contributions of A-D-PolyC. Firstly, we introduce polygon clipping for the identification of distinct lane change maneuvers on highways. The traffic scene topology is constructed based on relations between the obtained polygons and represented using a graph. Secondly, our approach directly considers the reachable set of the ego-vehicle and uses a clustering mechanism to reduce sample-complexity. Thirdly, we use geometric properties of the obtained polygons for the distribution of sample points in order to further reduce runtime. Finally, we employ scene prediction with an injected ego-vehicle trajectory to account for the influence of a lane change onto surrounding traffic. To quantify the effects, we developed a novel interaction cost based on generalized kinetic energies that is easy to interpret and parametrize.

III. Maneuver Identification

This section introduces the maneuver identification of A-D-PolyC, refer to the left part of Fig. 1. It consists of the transformation of the traffic scene to a Frenet-Serret-Frame, a scene analysis based on polygon clipping and the sample point generation.

A. Transformation to Frenet-Serret-Frame

The motivation to use a Frenet-Serret-Frame for automated driving is to exploit road structure. In this new coordinate frame, tube-like traffic scenes always appear as straight scenes so that unified handling of many different scenarios is achieved. The top left part of Fig. 2 shows an exemplary traffic scene with the ego-vehicle in dark blue and two traffic participants in light blue surrounding it on a curvy road. The ego vehicle coordinate frame is denoted by (X, Y). The coordinate frame origin of the Frenet-Serret-Frame, subsequently denoted as (L, N), is attached at $X = 0\,\mathrm{m}$ on the reference marking. The Lanelet transformation from [14] is used for the transformation of lane markings and predicted trajectories of surrounding traffic participants since transformed paths remain continuous and it was the fastest algorithm in a prior evaluation.

B. Lane-discrete spatiotemporal Free Space Description

One central contribution of A-D-PolyC is the polygon clipping in spatiotemporal domain to obtain lane change variants in a very efficient way. This corresponds to step ⓑ in Fig. 1. An illustration of the intersection of two polygons is shown in the middle part of Fig. 2. The operations intersection ($\cap$), union ($\cup$) and difference ($\setminus$) are applied using an adaption of Vattis polygon clipping algorithm [15].

Consider the top right part of Fig. 2. The light blue area is the ego lane space ahead and a rectangle in (L, t) domain, up to some limits $L_{\max}$ and $t_{\max}$ that the user of A-D-PolyC can configure. This is represented by the polygon:

$$P_{\mathrm{SL}} = \{(L_{\mathrm{SL},k}, t_{\mathrm{SL},k})_{k=0}^{n_{\mathrm{SL}}}\}, \tag{1}$$

where the subscript SL is short for start lane. A polygon is a closed polygonal chain of a set of points (L_k, t_k). On the current ego vehicle lane drives one traffic participant in front of it. If, for example, this vehicle drives with constant velocity $\dot{L}$, it occupies the dashed area in the (L, t) spatiotemporal domain on the ego lane in the lower right part of Fig. 2. This is mathematically represented by the polygon:

$$P_{\mathrm{OTP}} = \{(L_{\mathrm{OTP,k}}, t_{\mathrm{OTP,k}})_{k=0}^{n_{\mathrm{OTP}}}\}. \tag{2}$$

The subscript OTP is short for all other traffic participants of a scene, except the ego vehicle. Note that the slope in Fig. 2 (right) corresponds to the vehicles velocity. Safety margins can be directly accounted for by extending the vehicle's occupied area.

To get the free space on the ego lane, the difference operator ($\setminus$) is applied between the ego lane free space polygon and the traffic participant occupancy polygon:

$$\{P_i\} = P_{\mathrm{SL}} \setminus P_{\mathrm{OTP}}. \tag{3}$$

In the example, this results in two ($i \in \{1, 2\}$) distinct polygons P_1 and P_2 shown in the lower right part of the Fig. 2. The meaning of the upper area is, everything that is in front of the traffic participant in L and t. Similarly the lower part is the spatiotemporal free space behind the traffic participant and the ego vehicle resides at $(L = 0\,\mathrm{m}, t = 0\,\mathrm{s})$ within this second area at the start of a planning cycle.

TABLE I: Comparison of several state of the art approaches in the context of maneuver identification and planning for automated vehicles.

Approach	Planning horizon	Interaction-aware	Globalization strategy	Optimization method
Werling et al. [1]	10 s	No	Yes, via sampling	Uninformed sampling
Schlechtriemen et.al. [2]	Not described	No	Polylines	Informed sampling
Evested et al. [3]	10 s	Yes	Yes, via sampling	Uninformed sampling
Wei et al. [4]	15 s	Yes	Yes, via sampling	Uninformed sampling
Ardelt et al. [5]	Not described	No	None	Max. lane utility
Chen et al. [6]	Not described	No	Space-time exploration	Heuristic search
Ulbrich and Maurer [7]	14 s	Yes	ROI assesment	POMDP
Lenz et al. [8]	12 s	Yes	Inherently global approach	MCTS
Gu et al. [9]	6 s	No	DAG and pseudo H-signature	iLQR
Nilsson et.al. [10]	10 s	No	Gap selection heuristic	QP-MPC
Söntges and Althoff [11]	3 s	No	Reachable set propagation	None
A-D-PolyC (Ours)	10 s	Yes	Polygon clipping and graph	Informed sampling

Abbreviations: ROI: Region of interest, in this context corresponding to spatial areas around the ego-vehicle, POMDP: Partially Observable Markov Decision Process, MCTS: Monte-Carlo Tree Search, DAG: Directed Acyclic Graph, iLQR: iterative Linear Quadratic Regulator, QP: Quadratic Programming and MPC: Model Predictive Control. Note: Interaction-aware means for us that ego-vehicle decisions influence surrounding traffic decisions.

C. Spatiotemporal Scene Analysis using Polygon Clipping

Consider a straight traffic situation similar to the bottom left part of Fig. 2 and that a change to the left lane is issued by the mission planning. Applying the previously described method based on polygon clipping on the start lane and the target lane gives the enumerated lane free space areas shown in the left and middle $L{-}t$ diagrams in Fig. 3. Every number corresponds to a polygon in Fig. 3, for example:

$$① \mathrel{\hat{=}} P_1 = \{(L_{1,k}, t_{1,k})_{k=0}^{n_1}\}. \tag{4}$$

To reflect the fact, that there are three different types of areas, three index sets are introduced. In the example case:

$$\tilde{\mathcal{SL}} = \{1, 2\}, \quad \tilde{\mathcal{LC}} = \{3, 4, 5\}, \quad \tilde{\mathcal{TL}} = \{6, 7\}. \tag{5}$$

The set $\tilde{\mathcal{SL}}$ indexes spatiotemporal free space areas on the start lane of the ego vehicle, $\tilde{\mathcal{LC}}$ represents the lane change areas and $\tilde{\mathcal{TL}}$ is the index set of the areas on the target lane.

In order to identify maneuver variants, polygon clipping is utilized, this time applying the intersection ($\cap$) operator. The intersection of all areas of the start lane free space (① and ② in Fig. 3) with the free space areas in the target lane (⑥ and ⑦) are calculated. So for example $P_2 \cap P_6 = P_3$. This results in three distinct areas that are subsequently called lane change areas and indexed using the set $\mathcal{LC}$. Finally, the directed acyclic graph on the right in Fig. 3 is created that represents the connectivities of all obtained free space areas and therefore reflects the scene's topology. Since the ego vehicle starts in area ②, only two paths are actually traversable to get to the areas ③ and ⑤ on the target lane. Therefore the index sets can be further pruned:

$$\mathcal{SL} = \{2\}, \quad \mathcal{LC} = \{3, 5\}, \quad \mathcal{TL} = \tilde{\mathcal{TL}}. \tag{6}$$

The lane change areas denote spatiotemporal regions in $L{-}t$ in which both current and target lane are free, so a lane change is possible. To summarize, the ego vehicle starts in area ②. From there, it has the option to do a direct lane change in area ⑤ and to end up in front of the other traffic participant on the target lane in area ⑦. The other option is to first stay in area ② on it's lane, wait until the other traffic participant on the target lane passes the ego vehicle, conduct the lane change in area ③ and finally end up in area ⑥. That means that the ego vehicle is behind the traffic participant on the target lane at the end of the maneuver. The cycle at node ② corresponds to the trivial Adaptive Cruise Control (ACC) case that is active if there is no lane change request however not described here. Obtaining the maneuver variants is numerically easy and runtime bounded using Depth-first search in the graph.

D. Sample Point Generation exploiting the Scene Topology

In order to make A-D-PolyC sample efficient, next the geometric features of the lane change areas are analyzed. They are represented by the polygons P_3 and P_5. The starting point is the calculation of the reachable set $\mathcal{L}$ in $L{-}t$ considering maximum deceleration $\ddot{L}_{d,\max}$ and acceleration $\ddot{L}_{a,\max}$ starting from the current initial longitudinal velocity $\dot{L}_0$ of the ego vehicle:

$$L_u(t) = \int_{t=0}^{t_{\max}} \min\left(\dot{L}_o + \ddot{L}_{a,\max}\, t, \dot{L}_{\max}\right) \mathrm{d}t, \tag{7}$$

$$L_l(t) = \int_{t=0}^{t_{\max}} \max\left(\dot{L}_o + \ddot{L}_{d,\max}\, t, \dot{L}_{\min}\right) \mathrm{d}t, \tag{8}$$

with some situation dependent lower $\dot{L}_{\min}$ and upper bounds $\dot{L}_{\max}$ typically reflecting speed limits. The upper and lower

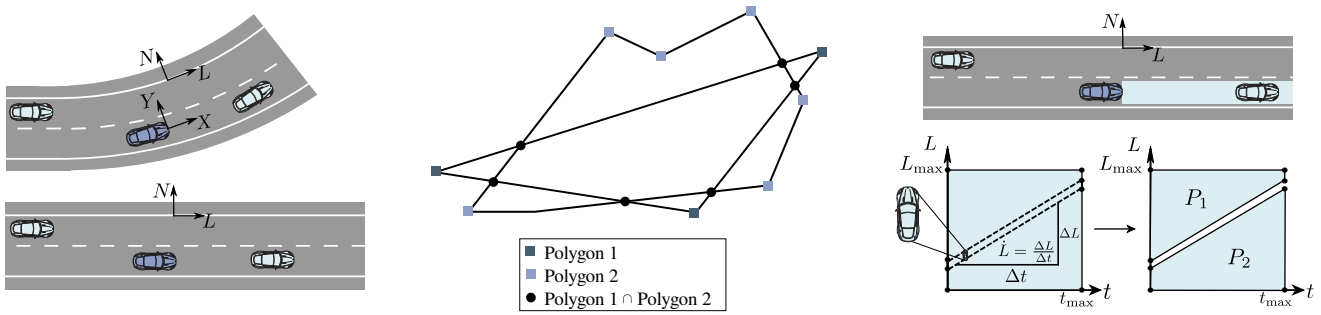

Fig. 2: Procedure to derive lanes free space areas. Left: Transformation of traffic scene into Frenet-Serret coordinate frame. Middle: Illustration of polygon clipping for intersection operation. Right: Lane free space derivation using polygon clipping.

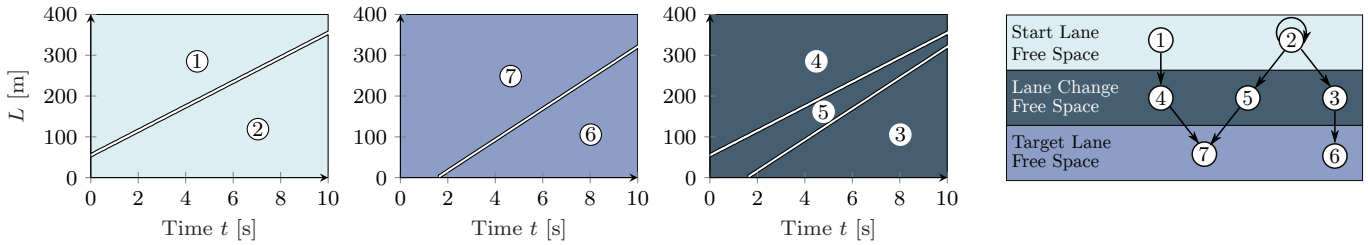

Fig. 3: First three figures correspond to spatiotemporal lane's free space areas. Each area ⓘ is represented using a polygon P_i. Left: Free space on current ego vehicle lane. Middle: Free space on left target lane. Right: Lane change areas, that correspond to free space simultaneously on current and target lane. Rightmost figure corresponds to the maneuver graph that encodes the traffic scene topology.

bound L_u and L_l are represented with polygonal chains. Closing them results in the dashed polygon $P_{\mathcal{L}}$ in the left column in Fig. 4. Applying the intersection operator ($\cap$) using polygon clipping results in modified, often smaller lane change areas $\hat{P}_3 = P_3 \cap P_{\mathcal{L}}$ and $\hat{P}_5 = P_5 \cap P_{\mathcal{L}}$. This way, sample-complexity is reduced. Next is the calculation of the spatiotemporal area of the modified lane change areas $\hat{P}_k$:

$$A_{\hat{\mathrm{P}}_k} = \frac{1}{2}\left(\sum_{i=0}^{n_i-1}\left(L_{\hat{\mathrm{P}}_k,i+1}\, t_{\hat{\mathrm{P}}_k,i} - L_{\hat{\mathrm{P}}_k,i}\, t_{\hat{\mathrm{P}}_k,i+1}\right)\right), k \in \mathcal{LC} \tag{9}$$

and the check if it is exceeding some user-defined threshold $A_{\min}$. Figuratively speaking, this means that the space and time that the ego vehicle has to conduct it's lane change is probably sufficient. This feature is used as a pruning heuristic to reduce the computational cost of A-D-PolyC. Next is the calculation of the equivalent height $L_{\mathrm{R},k}$ of a spatiotemporal rectangle with width $t_{\mathcal{LC},k}$ for the lane change areas of all maneuver variants:

$$L_{\mathrm{R,k}} = \frac{A_{\hat{\mathrm{P}}_k}}{t_{\mathcal{LC},k}}, k \in \mathcal{LC}. \tag{10}$$

Herein, $t_{\mathcal{LC},k}$ is the temporal extent of area $\hat{P}_k$. This feature is important when comparing two maneuver variants because the geometric shape of the lane change areas is a key aspect. Assuming two lane change areas with the same area A, it is often better to choose the one that has a longer time duration.

The final step consists of the generation of sample point sets within the lane change areas:

$$\mathcal{S}_k = \{S_j\}_{j=1}^{n_s},\ k \in \mathcal{LC} \tag{11}$$

with samples $S_j = \{(L_{j,\mathcal{SL}}, t_{j,\mathcal{SL}}), (L_{j,\mathcal{TL}}, t_{j,\mathcal{TL}})\}$ that the trajectories have to pass through. Herein n_{s} denotes the maximum number of samples. The times $t_{j,\mathcal{SL}}$ and $t_{j,\mathcal{TL}}$ correspond to the start and end of the ego-vehicle's lateral movement with the lane change duration $T_{\mathcal{LC}} = t_{j,\mathcal{TL}} - t_{j,\mathcal{SL}}$. Both $L_{j,\mathcal{SL}}$ and $L_{j,\mathcal{TL}}$ characterize the associated longitudinal coordinates of the start and end of the lateral movement. Then the centroids of the polygons $\hat{P}_k,\ k \in \mathcal{LC}$ are calculated. The calculation of the centroids $\left(C_{L,\hat{P}_k}, C_{t,\hat{P}_k}\right), k \in \mathcal{SL}$ is as follows:

$$A_{\hat{P}_k} = \frac{1}{2}\left(\sum_{i=0}^{n_{\hat{P}_k}-1}\left(L_{\hat{P}_k,i+1} t_{\hat{P}_k,i} - L_{\hat{P}_k,i}\, t_{\hat{P}_k,i+1}\right)\right), \tag{12}$$

$$\begin{aligned} C_{L,\hat{P}_k} = \frac{1}{6A_{\hat{P}_k}} &\sum_{i=0}^{n_{\hat{P}_k}-1}\left(L_{\hat{P}_k,i} + L_{\hat{P}_k,i+1}\right) \times \\ &\times \left(L_{\hat{P}_k,i+1}\, t_{\hat{P}_k,i} - L_{\hat{P}_k,i}\, t_{\hat{P}_k,i+1}\right), \\ C_{t,\hat{P}_k} = \frac{1}{6A_{\hat{P}_k}} &\sum_{i=0}^{n_{\hat{P}_k}-1}\left(t_{\hat{P}_k,i} + t_{\hat{P}_k,i+1}\right) \times \\ &\times \left(L_{\hat{P}_k,i+1}\, t_{\hat{P}_k,i} - L_{\hat{P}_k,i}\, t_{\hat{P}_k,i+1}\right). \end{aligned} \tag{13}$$

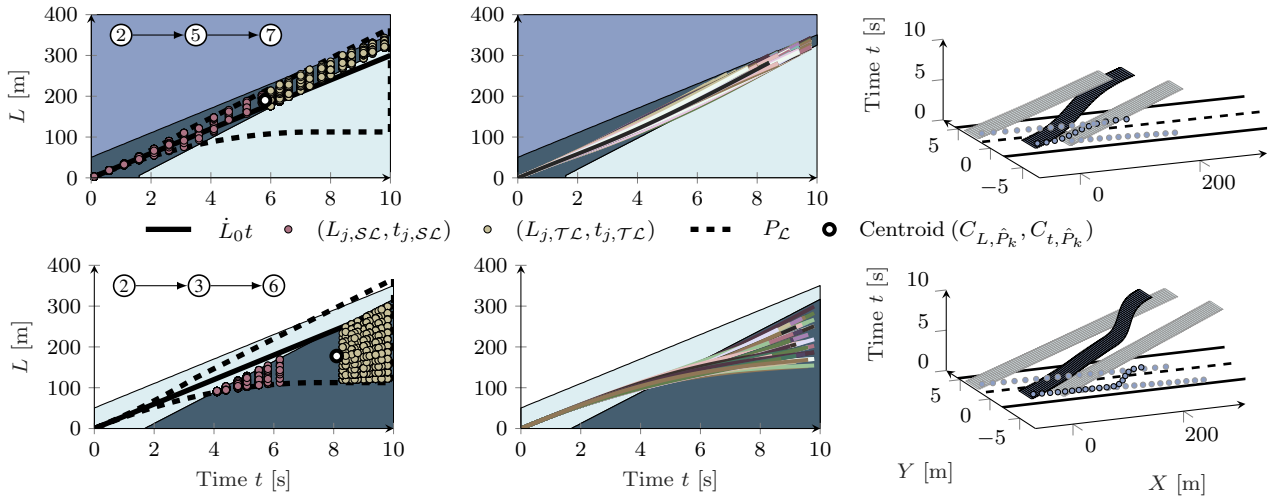

Fig. 4: A-D-PolyC procedure for direct (top row, ②→⑤→⑦) and indirect (bottom row, ②→③→⑥) lane change maneuver. Left: Sample points and reachable set. Middle: Calculated longitudinal trajectories. Right: Trajectory with minimum total cost J_{T} using $\lambda = 0.6$.

The centroids are represented in the left column of Fig. 4 using white dots. The time $C_{t,\hat{P}_k}$ of the centroid divides a lane change area naturally into two intervals:

$$I_{\hat{P}_k,1} = \left[t_{\hat{P}_k,\min}, C_{t,\hat{P}_k}\right), \quad I_{\hat{P}_k,2} = \left[C_{t,\hat{P}_k}, t_{\hat{P}_k,\max}\right], \quad (14)$$

where $t_{\hat{P}_k,\min}$ denotes the temporal beginning of the reachable lane change area and $t_{\hat{P}_k,\max}$ the ending. In case of direct lane change areas $t_{\hat{P}_k,\min} = 0\,\mathrm{s}$. For example, for area ③ the values are roughly $t_{\hat{P}_k,\min} = 1.8\,\mathrm{s}$ and $t_{\hat{P}_k,\max} = 10\,\mathrm{s}$ which is also the upper bound of our planning horizon. Then the intervals $I_{\hat{P}_k,1}$ and $I_{\hat{P}_k,2}$ are subdivided by a user-defined number of equidistant steps along the time axis, while omitting both boundaries. Finally, for every discrete time in both sets, a user-defined number of points between the upper and lower boundary of the intersection of the lane change area and the reachable set are sampled. The left column of Fig. 4 represents both sample sets $\mathcal{S}_3$ and $\mathcal{S}_5$.

Above mechanism generates a big number of meaningful samples. The absolute number is upper-bounded and the boundary depends on user-defined choices of interval subdivisions and number of points per time slice $t_{j,\mathcal{SL}}$ and $t_{j,\mathcal{TL}}$. Then several sanity checks for reducing the number of samples are conducted. For this, the mean longitudinal velocity $\overline{\dot{L}}_{\hat{P}_k,j}$ for every sample j is estimated by using a linear connection of the two associated points $(L_{j,\mathcal{SL}}, t_{j,\mathcal{SL}})$ and $(L_{j,\mathcal{TL}}, t_{j,\mathcal{TL}})$, that are shown in red and beige in the left column of Fig. 4. It is checked if this velocity is below the speed limit and also if the corresponding lane change has a duration of at least $T_{\mathrm{LC},\min} = 2.5\,\mathrm{s}$. Samples with a negative or zero mean velocity $\overline{\dot{L}}_{\hat{P}_k,j} \leq 0$ are removed, too. To ensure a deterministic upper boundary of the runtime of A-D-PolyC's trajectory calculation, it is necessary to have a fixed number of samples. It is intuitively clear, that an even distribution of samples within each maneuver variant's lane change area with regards to the mean velocities $\overline{\dot{L}}_{\hat{P}_k,j}$, end time of the lane change $t_{j,\mathcal{TL}}$ and final longitudinal coordinate $L_{j,\mathcal{TL}}$ for sets $\mathcal{S}_k,\ k \in \mathcal{LC}$ is desirable. K-Means clustering is used with a fixed number of iterations to cluster samples based on the above mentioned three attributes into a user-defined number of clusters. Then a user-defined number of samples is collected from each clusters. Consider one lane change area, represented by the polygon $\hat{P}_k$. Let $\dot{L}_{m_i}$, L_{m_i} and t_{m_i} denote and the mean longitudinal velocity, coordinate and end time of cluster i for this area. Let furthermore $L_{m_i,0} = L_{m_i} - \dot{L}_{m_i} t_{m_i}$ denote the L-axis intercept of cluster i. All clusters are sorted based on the euclidean distance:

$$d_i = \left\| \begin{bmatrix} L_{m_i,0} & \dot{L}_{m_i} \end{bmatrix}^\intercal - \begin{bmatrix} L_0 & \dot{L}_0 \end{bmatrix}^\intercal \right\|_2, \quad (15)$$

with the initial L coordinate L_0 and velocity $\dot{L}_0$. Most samples are chosen from clusters with the minimal distance d_i. This has the effect to guide the sampling such that the ego vehicle has the least need to change it's kinetic energy by decelerating or accelerating.

The output of the maneuver identification stage consists of the maneuver graph that encodes the traffic scene topology, spatiotemporal features and sample sets corresponding to each maneuver variant.

IV. Maneuver Assessment

This section introduces the maneuver assessment of A-D-PolyC. The goal is to calculate trajectories from the samples, check for feasibility and assign an interaction-aware cost to each.

A. Sampling of longitudinal and lateral Trajectories

The first step consists in the calculation of a set of candidate trajectories for all identified maneuver variants, refer to step ⓓ of Fig. 1. Methods from optimal control for trajectory generation are chosen to ensure comfort for the passengers. The lateral trajectory synthesis is based on [1] and formulated in a way to yield jerk-optimal lateral trajectories. To achieve this, fifth-order polynomials are used. As already mentioned in section III-C, lane change maneuver variants can be classified into direct and indirect lane changes. Intuitively, a direct lane change is the case if the ego vehicle can directly start to move laterally towards the target lane because the point $(L = 0\,\mathrm{m}, t = 0\,\mathrm{s})$ is in the lane change area. In the case of direct lane changes, only one segment $N_1(t)$ is used that takes the ego vehicle directly to the target lane with correct orientation with the lane's centerline. On the other hand, two segments are used for an indirect lane change. First, a trajectory segment $N_1(t)$ that orients the ego vehicle correctly with the start lane's centerline at the first sample point (red in left column of Fig. 4) is calculated. Afterwards a segment $N_2(t)$ that takes the ego vehicle to the target lane with correct orientation at the end of the maneuver is generated.

Our novel approach for the calculation of longitudinal trajectories is motivated by the work [16] for quadrotor flight. The main idea is to transform a constrained optimization problem into an unconstrained one to reduce computational cost and enhance numerical robustness. It is shown in [16] that a cost $J_L(T)$, penalizing the squares of the derivatives of the polynomial $L(t)$, for one single segment with duration T can be expressed in terms of the coefficients $\mathbf{p}_L \in \mathbb{R}^{n+1}$ of a n'th order polynomial of the segment and a final time dependent weight matrix:

$$J_L(T) = \mathbf{p}_L^\intercal \mathbf{Q}_L(T) \mathbf{p}_L, \quad (16)$$

$\mathbf{Q}_L \in \mathbb{R}^{(n+1)\times(n+1)}$. The order $n = 5$ is used. Refer to [16] for the construction of matrix $\mathbf{Q}_L$. A similar expression holds in the case of splines. We always use a spline consisting of two fifth order polynomials. The key idea then is to group the boundary constraints of the polynomials into free and fixed ones. Finally, the free constraints are optimized to obtain an optimal trajectory. Note that an unfixed planning horizon is used, that corresponds to the time $t_{j,\mathcal{TL}}$ of a sample. This gives A-D-PolyC more flexibility. Several generated longitudinal trajectories are shown in the middle column of Fig. 4 for both lane change maneuver variants.

B. Safety Check and Interaction-Aware Assessment of Maneuver Sample Trajectories

Next is the assessment of the generated trajectories. The goal is to find a fixed number of best trajectories for each maneuver

variant. A multi-stage optimization is used for this. Using the aforementioned scheme for the construction of the sample set $\mathcal{S}_k$, $k \in \mathcal{LC}$, calculation of trajectories $[L_j(t) \quad N_j(t)]^\intercal$ and transformation to the ego frame, we obtain the following set of trajectories:

$$\mathcal{T}_k = \{\boldsymbol{\tau}_j\}_{j=1}^{n_\mathcal{T}}, k \in \mathcal{LC}, \tag{17}$$

with a total of $n_\mathcal{T}$ trajectories $\boldsymbol{\tau}_j = [X_j(t) \quad Y_j(t)]^\intercal$. Our inner optimization problem is as follows:

$$\begin{aligned} &\min J_\mathrm{V}(\boldsymbol{\tau}_j), \text{ subject to:} \\ &\boldsymbol{\tau}_j \in (\mathcal{T}_\mathrm{CF} \cap \mathcal{T}_\mathrm{VC} \cap \mathcal{T}_\mathrm{OTPC} \cap \mathcal{T}_\mathrm{TR}), \end{aligned} \tag{18}$$

with the set $\mathcal{T}_\mathrm{CF}$ of collision free trajectories, the set $\mathcal{T}_\mathrm{VC}$ of trajectories that fulfill imposed vehicle dynamics and nonholonomic constraints. The differential flatness property of a kinematic nonlinear single-track model is used to check if wheel steering angles and rates fulfill box constraints. The set $\mathcal{T}_\mathrm{OTPC}$ consists of the trajectories that fulfill constraints on time gaps TG and time-to-collisions TTC to surrounding traffic and with $\mathcal{T}_\mathrm{TR}$, the set satisfying traffic rules like for example speed limits. Box constraints for $\mathcal{T}_\mathrm{OTPC}$ and for $\mathcal{T}_\mathrm{VC}$ are used and scaled with the urgency of the lane change. The cost functional is:

$$\begin{aligned} J_\mathrm{V} =& \omega_1|\ddot{X}_\mathrm{max}| + \omega_2|\ddot{Y}_\mathrm{max}| + \omega_3|X^{(3)}_\mathrm{max}| + \omega_4|\ddot{Y}^{(3)}_\mathrm{max}| + \\ &+ \omega_5\overline{|\ddot{X}|} + \omega_6\overline{|\ddot{Y}|} + \omega_7\overline{|X^{(3)}|} + \omega_8\overline{|Y^{(3)}|} + \\ &+ \omega_9\left(|\min(\dot{X}_\mathrm{TL}, \dot{X}_\mathrm{des}\right) - \dot{X}_\mathrm{T}|), \end{aligned} \tag{19}$$

with the empirically determined weighting factors $\omega_i \in \mathbb{R}$, maximum and mean absolute values $\overline{|\cdot|}$ of acceleration and jerk in X and Y direction, the estimated speed on the target lane $\dot{X}_\mathrm{TL}$, the desired velocity given by the mission planning $\dot{X}_\mathrm{des}$ and final ego vehicle velocity $\dot{X}_\mathrm{T}$. This results in an ordered set of $n_{\tilde{\mathcal{T}}}$ feasible trajectories $\tilde{\mathcal{T}}_k$, $k \in \mathcal{LC}$.

To account for interaction-awareness, we inject the feasible trajectories into a scene prediction engine [13] that uses the Intelligent Driver Model [17] and evaluate the reactions of all surrounding traffic participants. This reflects step ⓕ of A-D-PolyC in Fig. 1. We propose a new method to measure the interaction quantitatively. The idea is to use generalized kinetic energies. The ego vehicle and all other traffic participants have certain kinetic energies which are calculated based on initial predictions and that they ideally would maintain. It is therefore very intuitive to compare kinetic energies. However, one challenge that arises is the correct handling of big and heavy trucks. These would unbalance the calculation of the energies strongly. This is handled by using a normalized mass $\hat{m}$ that also accounts for the fact, that big trucks have stronger breaking systems and therefore are able to decrease kinetic energy stronger than passenger vehicles. We use the calculated trajectories in Frenet-Serret-Frame and obtain the expression:

$$\hat{E}(t) = \frac{1}{2}\hat{m}\left(\dot{L}^2(t) + \dot{N}^2(t)\right) \tag{20}$$

We propose to use $\hat{m}_P = 1\,\mathrm{kg}$ for passenger vehicles, $\hat{m}_M = 0.8\,\mathrm{kg}$ for motorbikes and $\hat{m}_T = 3\,\mathrm{kg}$ for trucks. In the second optimization loop, the aim is to minimize an interaction-aware cost functional J_I:

$$J_\mathrm{I} = \lambda\tilde{E}_\mathrm{ego} + (1-\lambda)\tilde{E}_\mathrm{OTP}. \tag{21}$$

The tilde ($\tilde{E}$) in equation (21) reflects the fact, that the values of the energies are normalized to always make them comparable to each other. Our approach benefits from good interpretability and there is only one parameter $\lambda \in \mathbb{R}$ that realizes the transition between cooperative and non-cooperative behavior. Subsequently, all steps needed to evaluate equation (21) are described and we begin by the formulation of several generalized kinetic energies for all $i \in \{0 \cup \mathcal{O}\}$ vehicles in traffic scene under consideration. The index $i = 0$ reflects the ego vehicle and the index set $\mathcal{O}$ all M traffic participants:

$$E_{i,\mathrm{prior}}(t) = \frac{1}{2}\hat{m}_{(\cdot)}\left(\dot{L}^2_{i,\mathrm{prior}}(t) + \dot{N}^2_{i,\mathrm{prior}}(t)\right), \tag{22}$$

$$E_{i,\mathrm{post}}(t) = \frac{1}{2}\hat{m}_{(\cdot)}\left(\dot{L}^2_{i,\mathrm{post}}(t) + \dot{N}^2_{i,\mathrm{post}}(t)\right), \tag{23}$$

$$\overline{|E_i|} = \frac{1}{n_i}\sum_{j=1}^{n_i}\max\left(0, E_{i,\mathrm{prior}}\left(t_j\right) - E_{i,\mathrm{post}}\left(t_j\right)\right) \tag{24}$$

$$\overline{|E_0|} = \frac{1}{n_0}\sum_{j=1}^{n_0}|E_{0,\mathrm{prior}}\left(t_j\right) - E_{0,\mathrm{post}}\left(t_j\right)| \tag{25}$$

$$E_\mathrm{OTP} \coloneqq \frac{1}{M}\sum_{i=1}^{M}|E_i|, \quad E_\mathrm{ego} \coloneqq \overline{|E_0|}, \tag{26}$$

with the number of timesteps n_i. The subscript prior reflects the situation if the ego vehicle would continue with it's initial velocity on the start lane. Special attention needs to be paid at the differences of the mean generalized energy calculation for other traffic participants and the ego vehicle in equations (24) and (25). Consider the case in which the ego vehicle conducts a lane change with the result that the vehicle on the start lane behind it can now drive faster and gain velocity. This results in $E_{i,\mathrm{prior}}(t_j) - E_{i,\mathrm{post}}(t_j) < 0$ such that the generalized energy is raised. A-D-PolyC should not punish such behavior and the $\max$ operator in (24) realizes that. The ego vehicle is handled differently and it is assumed, that it wants to keep it's initial generalized energy. This is accounted for by using the absolute value in equation (25). Notice, that this does not prohibit speeding up, since the cost functional in equation (19) of the previous optimization step puts weight on achieving the desired velocity.

A higher value of λ in equation (21) punishes changes of the normalized generalized kinetic energy of the ego vehicle more compared to the influence onto the surrounding traffic. This in turn leads to a more comfortable but non-cooperative ride. We expect to see lower values of jerk and accelerations but probably at the cost of lower time-to-collisions within the range of feasible TTCs. At the end, both cost functionals are normalized such that $\tilde{J}_\mathrm{V}, \tilde{J}_\mathrm{I} \in [0, 1]$ and the total cost formulated:

$$J_\mathrm{T} = \beta_1\tilde{J}_\mathrm{V} + \beta_2\tilde{J}_\mathrm{I}, \tag{27}$$

with weight factors $\beta_1, \beta_2 \in \mathbb{R}$.

TABLE II: Vehicle dynamics of the ego vehicle and situation features corresponding to both minimum J_{T} results in Fig. 4.

	$\max(\lvert\cdot\rvert)$				$\overline{\lvert\cdot\rvert}$				$\Delta\dot{X} = \dot{X}_{(\cdot)} - \dot{X}_{(\cdot)}$		$\min(TTC_{(\cdot)})$				Energies E	
Maneuver	$\ddot{X}$ $\frac{\mathrm{m}}{\mathrm{s}^2}$	$\ddot{Y}$ $\frac{\mathrm{m}}{\mathrm{s}^2}$	$X^{(3)}$ $\frac{\mathrm{m}}{\mathrm{s}^3}$	$Y^{(3)}$ $\frac{\mathrm{m}}{\mathrm{s}^3}$	$\ddot{X}$ $\frac{\mathrm{m}}{\mathrm{s}^2}$	$\ddot{Y}$ $\frac{\mathrm{m}}{\mathrm{s}^2}$	$X^{(3)}$ $\frac{\mathrm{m}}{\mathrm{s}^3}$	$Y^{(3)}$ $\frac{\mathrm{m}}{\mathrm{s}^3}$	T-0 $\frac{\mathrm{m}}{\mathrm{s}}$	T-des $\frac{\mathrm{m}}{\mathrm{s}}$	CB s	CF s	TB s	TF s	OTP J	Ego J
②→⑤→⑦	1.49	0.68	2.47	1.13	0.87	0.42	0.44	0.43	5.24	1.91	∞	14.46	19.57	∞	22.39	100.28
②→③→⑥	2.64	1.59	4.6	4.20	1.38	0.44	0.93	0.72	0.42	-2.93	∞	∞	∞	∞	0	80.36

Abbreviations: T-0: Longitudinal velocity difference between ego velocity at beginning and end of lane change, T-des: Long. vel. diff. between ego velocity at end of lane change and desired velocity (here: speed limit on target lane), SB: Start lane, behind ego vehicle, SF: Start lane, in front of ego vehicle, TB: Target lane, behind ego vehicle, TF: Target lane, in front of ego vehicle, OTP: Other traffic participants.

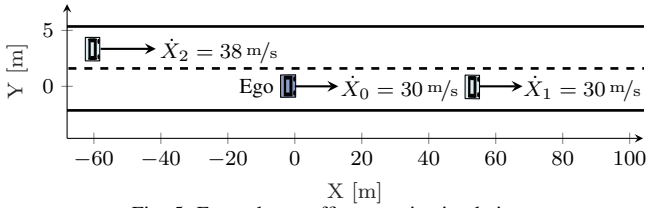

Fig. 5: Exemplary traffic scene in simulation.

V. Experiments and Evaluation

The scenario under consideration is the running example in this contribution, refer to Fig. 5. We use the simulation environment described in [18] that takes into account uncertain measurements of the vehicles sensors and provides the correct data structures that allows the quick deployment of developed algorithms. Let $X_1(t)$ and $\dot{X}_1(t)$ denote the longitudinal coordinate and velocity of the traffic participant on the target lane behind and $X_2(t)$ and $\dot{X}_2(t)$ on the start lane in front of the ego vehicle. Now the initial values of the longitudinal coordinate and velocity of the vehicle on the target lane are randomized by sampling from uniform probability distributions, $X_{2,0} \sim U(-85\,\mathrm{m}, -25\,\mathrm{m})$ and $\dot{X}_{2,0} \sim U(27.5\,\frac{\mathrm{m}}{s}, 46.5\,\frac{\mathrm{m}}{s})$. The longitudinal velocities of the ego vehicle and the traffic participant in front of it are always fixed to $\dot{X}_{\mathrm{ego}}(t) = \dot{X}_1(t) = 30\,\frac{\mathrm{m}}{\mathrm{s}}$. For the ego vehicle's desired velocity, the value $\dot{X}_{\mathrm{des}} = 33.3\,\frac{\mathrm{m}}{\mathrm{s}}$ is used. The evaluation of A-D-PolyC is done with a focus on the introduced interaction-aware quality measure introduced in the last section. A total of 500 simulation runs are used for the evaluation. The histograms in Fig. 6 show two critical features, the minimum time-to-collision $TTC_{\min}$ and the mean longitudinal acceleration $\overline{\ddot{X}}_{\mathrm{ego}}$ of the ego vehicle. They show that a high λ tends to result in lower mean longitudinal acceleration since changes of kinetic energy that correspond to ego-velocity changes are stronger punished. A side effect of this is, that the TTCs are also lowered, resulting in a more egoistic behavior.

The right column of Fig. 4 shows the best trajectories in (X, Y, t) domain for both maneuver variants for one simulation run corresponding to the configuration shown in Fig. 5. The table II shows a subset of the calculated features. The factor $\lambda = 0.6$ was used for generating these results. The rows in table II correspond to both identified maneuver variants. It might be somewhat surprising that the maximum and mean values of acceleration and jerk in both directions X and Y are higher in the second maneuver in which the ego vehicle waits to merge behind the faster vehicle that comes from the back on the target lane. The explanation for this lies in the fact, that we look at the first planning cycle at $t = 0\,\mathrm{s}$ and work with a fixed maximum time horizon of $t_{\max} = 10\,\mathrm{s}$ in which the lane change has to be conducted. Looking at the traffic scene, refer to Fig. 5, it is obvious that the ego vehicle has several options that are traded-off by the weighting factors in equations (19), (21) and (27). Since the weight ω_9 in equations (19) is comparably high to the other weights, the ego vehicle prefers a lane change where it first breaks slightly to reduce it's velocity to afterwards change lane and during the lane change speed up to achieve the target velocity. The lane change duration for this is short and therefore the lateral dynamics are also higher compared to the direct lane change in row 1 of table II. Considering the generalized, unnormalized energies E_{OTP} and E_{Ego}, it can be seen that the influence of maneuver ②→⑤→⑦ onto the surrounding traffic is stronger than it is for maneuver ②→③→⑥. Note, that the accompanying video to this contribution illustrates the results of our proposed framework in more complex highway traffic scenarios with more surrounding traffic participants and curves.

Finally, our trajectory generation approach is compared to the state-of-the-art method described in [10] which is based on a quadratic programming model-predictive control formulation. Refer to [10] for a description of the cost function and parameter values. We reimplemented the approach to work with the data from our scene prediction engine. The constraints for longitudinal and lateral acceleration and jerk from [10] are also used in A-D-PolyC to make the results comparable. Furthermore, we aim to minimize the interaction cost J_I in equation (21) via using the parameter $\lambda = 0$ in equation (21). Again, the example scene in Fig. 5 with parametrization $\{X_0 = 0\,\mathrm{m}, \dot{X}_0 = 33.3\,\frac{\mathrm{m}}{\mathrm{s}}, X_1 = 150\,\mathrm{m}, \dot{X}_1 = 33.3\,\frac{\mathrm{m}}{\mathrm{s}}, X_2 = -70\,\mathrm{m}, \dot{X}_2 = 37\,\frac{\mathrm{m}}{\mathrm{s}}\}$ is used. Since the first optimization

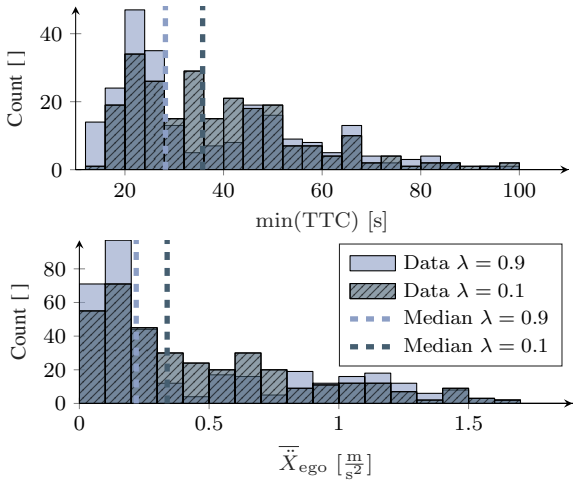

Fig. 6: Histogram and median values of $TTC_{\min}$ (top) and $\overline{\ddot{X}}$ (bottom) for $\lambda = 0.1$ and $\lambda = 0.9$.

TABLE III: Comparison of our approach to [10] using a total of 100 runs of A-D-PolyC to evaluate the non-deterministic k-means clustering.

Approach	$\overline{\lvert\ddot{X}\rvert}$ $\frac{\mathrm{m}}{\mathrm{s}^2}$	$\overline{\lvert\ddot{Y}\rvert}$ $\frac{\mathrm{m}}{\mathrm{s}^2}$	$\overline{\lvert X^{(3)}\rvert}$ $\frac{\mathrm{m}}{\mathrm{s}^3}$	$\overline{\lvert Y^{(3)}\rvert}$ $\frac{\mathrm{m}}{\mathrm{s}^3}$	$\min(TTC_{\mathrm{TB}})$ s	E_{OTP} J
A-D-PolyC						
(μ)	0.44	0.14	0.18	0.09	26.76	2.06
(σ^2)	9.6e-3	7.1e-4	2.9e-3	8.2e-4	18.21	2.91
Nilsson et al. [10]	0.26	0.12	0.18	0.10	18.02	13.80

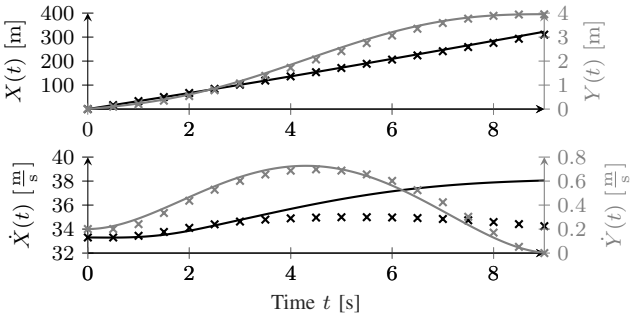

Fig. 7: Comparison of A-D-PolyC's ego-vehicle trajectories to the direct optimization approach of Nilsson et al. [10]. The crosses correspond to Nilsson et al.'s and the solid lines to our approach. Gray color is used to represent velocities and black for positions.

stage of A-D-PolyC aims to maximize ride comfort, above parameters are a sensible choice. Fig. 7 shows the obtained positions and velocity of both approaches. We used a trajectory to represent our approach that corresponds well to the mean values in table III. It can be seen that the results are comparable with respect to ride comfort, especially for the lateral movement. Since k-means clustering is used, we report the mean μ and variance σ^2 of the quantities. The key difference is that A-D-PolyC prefers to speed up in order to minimize interaction cost such that the traffic participant on the target lane has to break less compared to the result of the reimplementation of [10]. This can be seen by inspection of E_{OTP} and $\min(TTC_{(\mathrm{TB})})$ in table III. However, we want to highlight, that the work [10] incorporates a hard constraint on timegaps to surrounding traffic. Trajectories therefore maintain safe distances with respect to the fixed initial trajectory predictions of the surrounding traffic. However, there is no feedback to measure the influence of a planned trajectory onto traffic. In comparison our approach has an advantage, since it closes the feedback loop by injecting planned trajectories into the scene prediction to account directly for interactions. Furthermore, using a sampling approach has the advantage in safety critical situations when the optimizer is not able to provide a solution because of violated hard constraints. In such situations, using A-D-PolyC, one is able to still choose the trajectory that corresponds to the minimum global cost. This is also the reason why sampling approaches are often used as a redundancy layer in complex motion planning systems.

VI. Conclusions and Future Work

The current state of the A-D-PolyC framework was introduced. It solves the problem of lane change behavior planning using informed, meaningful sampling of trajectories while exploiting the spatiotemporal traffic scene topology efficiently using polygon clipping. MATLAB is used in the current prototyping phase. However, the next step is the realization of a parallelized and optimized implementation using CUDA-C and an extensive runtime analysis. In the design phase of A-D-PolyC, much care was taken to ensure numerical robustness and efficiency, clever pruning strategies and runtime boundedness. It is expected that runtimes can be achieved that are fast enough for an online behavior planning algorithm. We are furthermore currently working on generalizing the maneuver identification stage of A-D-PolyC to handle lane change maneuvers of surrounding traffic participants correctly. Finally, we are planning to couple the framework with an optimization based local motion planner and to make the transition from simulation to the test vehicle in the near future.

References

[1] M. Werling, J. Ziegler, S. Kammel, and S. Thrun, "Optimal trajectory generation for dynamic street scenarios in a frenet frame," in *IEEE Intl. Conference on Robotics and Automation*, May 2010.

[2] J. Schlechtriemen, K. P. Wabersich, and K. D. Kuhnert, "Wiggling through complex traffic: Planning trajectories constrained by predictions," in *IEEE Intelligent Vehicles Symposium*, June 2016.

[3] N. Evestedt, E. Ward, J. Folkesson, and D. Axehill, "Interaction aware trajectory planning for merge scenarios in congested traffic situations," in *IEEE Intl. Conference on Intelligent Transportation Systems*, Nov. 2016.

[4] J. Wei, J. M. Snider, T. Gu, J. M. Dolan, and B. Litkouhi, "A behavioral planning framework for autonomous driving," in *IEEE Intelligent Vehicles Symposium*, June 2014.

[5] M. Ardelt, C. Coster, and N. Kämpchen, "Highly automated driving on freeways in real traffic using a probabilistic framework," *IEEE Transactions on Intelligent Transportation Systems*, vol. 13, no. 4, pp. 1576–1585, Dec. 2012.

[6] C. Chen, M. Rickert, and A. Knoll, "Kinodynamic motion planning with space-time exploration guided heuristic search for car-like robots in dynamic environments," in *IEEE Intl. Conference on Intelligent Robots and Systems*, Sep. 2015.

[7] S. Ulbrich and M. Maurer, "Towards tactical lane change behavior planning for automated vehicles," in *2015 IEEE 18th International Conference on Intelligent Transportation Systems*, Sep. 2015.

[8] D. Lenz, T. Kessler, and A. Knoll, "Tactical cooperative planning for autonomous highway driving using monte-carlo tree search," in *2016 IEEE Intelligent Vehicles Symposium (IV)*, June 2016.

[9] T. Gu, "Improved trajectory planning for on-road self-driving vehicles via combined graph search, optimization & topology analysis," Ph.D. dissertation, Carnegie Mellon University, 2017.

[10] J. Nilsson, M. Brännström, E. Coelingh, and J. Fredriksson, "Lane change maneuvers for automated vehicles," *IEEE Transactions on Intelligent Transportation Systems*, vol. 18, no. 5, pp. 1087–1096, May 2017.

[11] S. Söntges and M. Althoff, "Computing the drivable area of autonomous road vehicles in dynamic road scenes," *IEEE Transactions on Intelligent Transportation Systems*, vol. 19, no. 6, pp. 1855–1866, June 2018.

[12] P. Bender, Ö. Ş. Taş, J. Ziegler, and C. Stiller, "The combinatorial aspect of motion planning: Maneuver variants in structured environments," in *IEEE Intelligent Vehicles Symposium*, June 2015.

[13] C. Wissing, T. Nattermann, K. Glander, and T. Bertram, "Interaction-aware long-term driving situation prediction," in *IEEE Intl. Conference on Intelligent Transportation Systems*, Nov. 2018.

[14] P. Bender, J. Ziegler, and C. Stiller, "Lanelets: Efficient map representation for autonomous driving," in *IEEE Intelligent Vehicles Symposium*, June 2014.

[15] B. R. Vatti, "A generic solution to polygon clipping," *Commun. ACM*, vol. 35, no. 7, pp. 56–63, Jul. 1992.

[16] C. Richter, A. Bry, and N. Roy, "Polynomial trajectory planning for quadrotor flight," in *IEEE Intl. Conference on Robotics and Automation*, May 2013.

[17] M. Treiber, A. Hennecke, and D. Helbing, "Congested traffic states in empirical observations and microscopic simulations," *Physical Review*, vol. 62, pp. 1805–1824, Feb. 2000.

[18] C. Wissing, T. Nattermann, K. Glander, A. Seewald, and T. Bertram, "Environment simulation for the development, evaluation and verification of underlying algorithms for automated driving," in *AmE 2016 - Automotive meets Electronics; 7th GMM-Symposium*, March 2016.